2016

Ferroelectric polymer nanopillar arrays on flexible substrates by reverse nanoimprint lithography

Jingfeng Song
University of Nebraska-Lincoln, jsong4@unl.edu

Haidong Lu
University of Nebraska-Lincoln, s-hlu4@unl.edu

Keith Foreman
University of Nebraska-Lincoln, keith.foreman@unl.edu

Shumin Li
University of Nebraska-Lincoln, sli12@unl.edu

Li Tan
University of Nebraska - Lincoln, ltan4@unl.edu

See next page for additional authors

Authors
Jingfeng Song, Haidong Lu, Keith Foreman, Shumin Li, Li Tan, Shireen Adenwalla, Alexei Gruverman, and Stephen Ducharme

Journal of
Materials Chemistry C

PAPER

View Article Online
View Journal

Cite this: DOI: 10.1039/c6tc01848c

Ferroelectric polymer nanopillar arrays on flexible substrates by reverse nanoimprint lithography†

Jingfeng Song,*[a] Haidong Lu,[a] Keith Foreman,[a] Shumin Li,[b] Li Tan,[b] Shireen Adenwalla,[a] Alexei Gruverman[a] and Stephen Ducharme*[a]

Received 5th May 2016,
Accepted 26th May 2016

DOI: 10.1039/c6tc01848c

www.rsc.org/MaterialsC

With the increasing interest in deploying ferroelectric polymer in flexible electronics and electro-mechanics, high-throughput and low-cost fabrication of 3D ferroelectric polymer nanostructures on flexible substrates can be a significant basis for future research and applications. Here, we report that large arrays of ferroelectric polymer nanopillars can be prepared directly on soft, flexible substrates by using low-cost polydimethylsiloxane (PDMS) soft-mold reverse nanoimprint lithography at 135 °C and at pressures as low as 3 bar. The nanopillar arrays were highly uniform over large areas of at least 200 × 200 μm and had good crystallinity with nearly optimum (110) orientation. Furthermore, the method leaves little or no residual polymer layer, fully isolating the nanopillars to avoid cross-talk and, obviating the need for additional etching processes that arises with conventional low-contrast nanoimprinting. The ferroelectric properties of individual nanopillars were probed by piezoresponse force microscopy, which showed that they exhibited switchable and bi-stable polarization. In addition, the polarization hysteresis loops probed by pyroelectric measurements of the entire array showed that the nanopillar capacitor arrays had good ferroelectric switching characteristics, over areas of at least 1 mm × 1 mm.

Introduction

Ferroelectric polymer nanostructures are of great interest due to their potential use in a wide range of applications, such as organic electronics,[1,2] electro-mechanics,[3,4] nonvolatile memories,[5–8] and solid-state energy storage, harvesting and conversion.[9–12] With the increasing application of ferroelectric polymers in the area of flexible electronics,[13–16] high-throughput and low-cost fabrication of uniform ferroelectric polymer nanostructures with good ferroelectric properties over large areas on flexible substrates will be a significant basis for flexible electronics applications. Previous studies of ferroelectric polymers, like polyvinylidene-*co*-trifluoroethylene, P(VDF–TrFE), report results from conventional nanoimprint lithography (NIL) with high-cost rigid molds at high pressures ranging from 20 bar to 120 bar and 130 to 150 °C to produce ferroelectric nanostructures on hard substrates.[5,7,17–21] Application of conventional NIL to produce nanostructured films on flexible substrates has a number of drawbacks, such as mechanical and thermal deformation of the substrates,[22,23] poor adhesion,[24] and incompatibility with high temperatures.[25,26] These drawbacks lead to low throughput and poor pattern uniformity in large arrays.[27,28] In addition, the conventional nanoimprint procedure usually requires an additional etching process to remove a residual polymer layer left between the imprinted structures.[29,30] This extra etching process may also be incompatible with flexible substrates due to their poor etching resistance.[31] Previous research on reverse nanoimprinting, where the material is first coated onto rigid mold and then transferred onto the substrate, has demonstrated the possibility of preparing high quality gratings of amorphous poly(methyl methacrylate) on both silicon substrates and on flexible polyimide films.[32]

Based on these considerations, we have developed a PDMS soft-mold based low-pressure reverse nanoimprint lithography (reverse NIL) process for preparing 3D ferroelectric polymer nanostructures on flexible substrates.[33] The specific benefits of this process are as follows: it is based on the use of PDMS soft molds that are low-cost, easily replicable, and highly customizable.[28,34–36] Furthermore, they often do not require surfactant pretreatment, as opposed to expensive pretreated rigid molds; the soft, non-sticking, PDMS mold enables conformal contact with the substrates even at very low pressures,[30,36] which makes it compatible with flexible substrates coated with conductive thin film bottom electrodes; it leaves little or no residual layer, fully isolating the nanopillars to avoid cross-talk and additional etching process that arise with conventional low-contrast nanoimprinting.

[a] Department of Physics and Astronomy & Nebraska Center for Materials and Nanoscience, University of Nebraska, Lincoln, NE 68588-0299, USA. E-mail: jingfsong@huskers.unl.edu, sducharme1@unl.edu
[b] Department of Mechanical and Materials Engineering & Nebraska Center for Materials and Nanoscience, University of Nebraska, Lincoln, NE 68588-0526, USA

† Electronic supplementary information (ESI) available: The supplementary information describes additional features of the nanopillar arrays and capabilities of the reverse nanoimprint lithography method. See DOI: 10.1039/c6tc01848c

Here, we report the results of a study of the application of low pressure, soft mold, reverse NIL to make regular arrays of ferroelectric nanopillars of P(VDF–TrFE) on substrates of polyethylene terephthalate (PET) coated with indium-tin-oxide (ITO) electrodes. Our results demonstrate that the P(VDF–TrFE) nanopillar arrays were faithful and uniform replicas of the PDMS mold over large areas of at least 200 μm × 200 μm, with no detectable residual layer. The nanopillar arrays were found to be predominantly in the ferroelectric phase at room temperature, with good crystallinity and uniform (110) orientation (polarization axis 30° from normal). The ferroelectric properties of individual nanopillars were probed by piezoresponse force microscopy, which showed that they exhibited switchable and bi-stable polarization. The polarization hysteresis loops probed by pyroelectric measurements demonstrated that the arrays of nanopillar capacitors had good ferroelectric switching characteristics, over areas of at least 1 mm × 1 mm. The reverse NIL method described here is a high-yield, low cost, scalable, and highly customizable method that provides a promising alternative to the traditional rigid-mold direct nanoimprinting processes. This method may serve as a significant basis for future studies of 3D functional polymer nanostructures for application in flexible electronics, electromechanics and energy harvesting applications.

Experimental

Preparation of PDMS soft mold and substrates

The PDMS molds were prepared from commercial silicon nanostamps that were obtained from LightSmyth Technologies, Inc. (Eugene, OR). The silicon nanostamps were 9 mm × 9 mm in size and consisted of nanopillars 200 nm in width and 150 nm in height and a period of 600 nm in rectangular or hexagonal arrangements. The silicon nanostamps were first cleaned with oxygen plasma in a Trion Minilock-Phantom III Reactive Ion Etching (RIE) system for 10 min, then immersed in a solution of 0.5 mM perfluorodecyltrichlorosilane in heptane for 1 min in order to form a thin surfactant layer over the mold surface, to facilitate release from the silicon mold. The PDMS precursor was prepared from the Sylgard 184 silicon elastomer kit by mixing 40 g of Sylgard 184 base with 4 g of curing agent. The mixed PDMS was then cast onto the surfactant-treated silicon master mold on a Petri dish and placed under vacuum at a pressure of 90 kPa for 30 min to remove bubbles generated during the mixing process. The PDMS molds were then cured in a convection oven set to 100 °C for 1 h and then carefully peeled off from the silicon master molds and cut to areas of 1 cm × 1 cm respectively. The PDMS replication process did not alter or damage the silicon master molds, and at least 20 replicas could be made with one single of surfactant treatment of the silicon master mold.[37] The PET substrates coated with ITO from Delta Technologies were cut into sizes of 1 cm × 1 cm and washed with dry acetone. To enhance the adhesion of P(VDF–TrFE) to the substrates, the PET substrates were modified by immersing them into a 0.1 M solution of aminopropyltriethoxysilane in dry acetone at 60 °C for 10 min.[5]

Fabrication of nanopillar array and capacitors

The PDMS molds were coated with a P(VDF–TrFE) copolymer thin film using the Langmuir–Blodgett (LB) deposition method. The copolymer of vinylidene fluoride (70%) and trifluoroethylene (30%), P(VDF–TrFE), from Kunshan Hisense Electronics Co., Ltd, was used as received and dissolved in dimethylsulfoxide to a concentration of 0.05% by weight. The thin film of 5 nominal monolayers, which has been proved to be suitable for forming continuous thin layer on the mold and effectively removing residual polymer layer after imprinting,[30,33,38] was transferred to the mold surface by horizontal Langmuir–Blodgett (LB) deposition at a surface pressure of 5 mN m^{-1}. The method of sample preparation and the properties of the produced films are described in greater detail elsewhere.[39,40]

The fabrication procedure for the P(VDF–TrFE) nanopillar arrays is illustrated in Fig. 1a. A polymer-coated PDMS mold was placed face-down on top of the ITO-coated PET substrate and heated to 135 °C, which has been found to be the optimum temperature to promote nanocrystalline self-assembly of P(VDF–TrFE).[41] The mold was pressed onto the substrate with a hydraulic press (SPECAC) at pressures ranging from 3 bar to 2.6 bar for 1 hour (see ESI†). The system was then cooled down to room temperature within 90 minutes, at which time the pressure was released and sample and mold were separated.

The multilayer nanopillar array capacitors for pyroelectric hysteresis measurements were fabricated directly on PET substrates as follows. The clean PET substrate was first coated with a 30 nm thick Pt film followed by a 30 nm thick MgO film, both deposited by sputtering through a shadow mask as bottom electrode. The PET substrates were immersed into a 0.1 M solution of aminopropyltriethoxysilane surfactant in dry acetone at 60 °C for 10 min.[5] The thin MgO layer was used for enhancing adhesion between the nanopillars and the substrate. The nanopillars were then imprinted onto the PET substrate. Next, the nanopillars

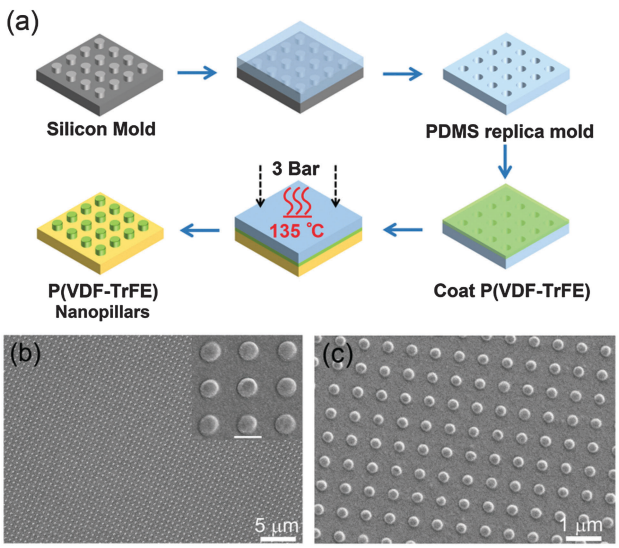

Fig. 1 (a) The procedure for preparation of the PDMS soft mold and reverse nanoimprint lithography. (b) and (c) The SEM images of the P(VDF–TrFE) nanopillars with a scale bar of 500 nm in the inserted image in (b).

were coated with 45 monolayers of a P(VDF–TrFE–CFE) terpolymer capping layer through LB deposition. The terpolymer capping layer, which has high dielectric constant, little remnant polarization and negligible pyroelectric response compared with P(VDF–TrFE) copolymer,[42–44] was chosen to prevent short-circuit and to share less voltage drop across the multilayer capacitor during the DC poling process (see ESI†). The terpolymer-coated nanopillar sample was then covered with a 100 nm thick aluminum top electrode by thermal evaporation through a shadow mask. The area of the nanopillar capacitor was 1 mm × 1 mm.

Morphology and structural characterization

The surface morphology of the copolymer nanopillar arrays was imaged by scanning electron microscopy (SEM, Hitachi model S4700 Field-Emission microscope) with an acceleration voltage of 2 kV. The 1 cm × 1 cm sample was pre-coated with a 5 nm thick gold layer by sputtering to reduce charging. The topography of the nanopillar arrays was measured with an Asylum Research MFP-3D atomic force microscope (AFM) using platinum-coated cantilevers (Mikromasch, CSC17/Pt) in a tapping mode at a frequency of 100 kHz and a modulation amplitude of 1 V.

The crystal structure of the imprinted nanopillars was studied by X-ray diffraction (XRD) measurement using a Panalytical Empyrean diffractometer with the Cu-K_α line (1.54 Å). The sample was mounted on a spinning stage with speed of 0.25 rpm and the out-of-plane (θ–2θ mode) diffraction signals were collected with 2θ ranging from 17° to 21° at a step size of 0.013°. The XRD data was fitted to a Lorentzian line shape function using Origin 9.0.[45]

Characterization of ferroelectric properties

The Piezoresponse Force Microscopy (PFM) images of the out-of-plane piezoelectric response of the individual nanopillars were carried out in contact mode using the high-voltage PFM module of Asylum Research MFP-3D AFM and an AC 240 TM cantilever made of a tetrahedral silicon tip coated with platinum/titanium in a resonant-enhanced mode at a frequency of 170 kHz and a modulation amplitude of 0.8 V. The sample polarization was altered at specific locations with the tip in contact while applying a DC tip bias of up to ±20 V. The PFM imaging was conducted in tapping mode in a back-and-forth pattern that that corresponds to the horizontal axis in all of the images. The local PFM hysteresis loops were obtained by holding the PFM tip at fixed locations and cycling the DC applied voltage in the range of ±15 V while recording the PFM phase and amplitude signals as a function of the DC bias (the PFM tip itself served as the top electrode, while the ITO coating served as bottom electrode).

The pyroelectric hysteresis loops of the nanopillar capacitors were measured using the rapid laser modulation heating method (Chynoweth method).[46] The nanopillar capacitor was heated through the Al top electrode by a 20 mW, 2 mm diameter blue diode laser beam chopped at frequency of 1.5 kHz. The pyroelectric current was measured using an SR830 lock-in amplifier with a 300 ms time constant referenced to the chopper frequency. Hysteresis loops were obtained by recording the pyroelectric signal as a function of DC bias between ±40 V with step size of 1 V. At each step, the bias voltage was held constant for 5 min and then removed during brief measurement. This latter precaution eliminates contributions to the pyroelectric signal due to the thermal expansion and the temperature dependence of the dielectric constant.[47]

Results and discussion

The nanopillar array is very uniform over a large area of 40 μm × 30 μm with few defects, as is shown from the SEM images of the P(VDF–TrFE) nanopillars in Fig. 1b and c. Furthermore, the clean and smooth surface morphology between the nanopillars indicated no residual layer of P(VDF–TrFE) copolymer left on the substrate between the nanopillars after imprinting. The individual sizes of the P(VDF–TrFE) copolymer nanopillars were studied in detail *via* AFM topography and line scan profile measurement with the results shown in Fig. 2a. The reverse NIL process yielded cylindrical copolymer nanopillars 88 ± 5 nm in height, 657 ± 12 nm in period, and an average of 245 ± 4 nm from the top and bottom widths. Studies of nanostructure self-assembly on a silicon substrate (without a mold) at atmospheric pressure and 135 °C with the same ferroelectric copolymer show that it readily dewets from the substrate in favor of nanomesas with excellent ferroelectric properties, this process is facilitated by the liquid-like condis nature of the paraelectric phase.[41] The main distinction here is that the mold determines the precise pattern of the nanopillars and therefore ensures precise and directed self-assembly. This is also why it works at such a low pressure of 3 bar, just enough to ensure intimate contact between mold and substrate. In addition, the hydrophobic surface of the PDMS mold enabled easy separation and smooth surface of the copolymer nanopillars. This hydrophobic property is another advantage of using the PDMS soft molds compared to previous work with rigid molds that require surface pretreatment for smooth separation after imprinting.[5,18,32,48]

The crystal structure of the P(VDF–TrFE) nanopillars imprinted on PET was characterized by out-of-plane X-ray diffraction (XRD). The XRD data of the nanopillar array sample shown in Fig. 2b (black dots) was fitted to a Lorentzian line-shape function (red curve, Fig. 2b) with a peak at 2θ = 19.66° ± 0.02, which coincides with the (110) reflection of the ferroelectric beta

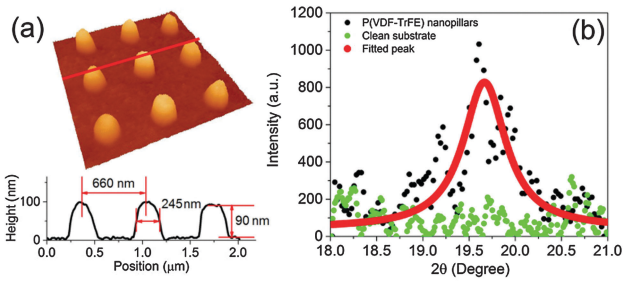

Fig. 2 (a) AFM topography of the P(VDF–TrFE) nanopillars and the line scan profile along the red line shown on the topography image. (b) Out of plane XRD result of the clean PET substrate (green dots) and the P(VDF–TrFE) nanopillars on PET substrate (black dots) and the fitted Lorentzian-shaped diffraction peak (red curve).

phase of the copolymer. No indication of paraelectric alpha phase of the copolymer was observed, as there was no obvious peak at $2\theta = 18.1^\circ$.[49] The dip at 19.4° from the XRD data of the nanopillars in Fig. 2b could be due to the noise during the measurement. The XRD data from the PET substrate (green dots, Fig. 2b), which was measured under the same conditions shows only a background signal in this range. The XRD measurements, therefore, show that the PDMS soft-mold based reverse nanoimprint method conducted at a low pressure of 3 bar and a temperature of 135 °C was able to prepare ferroelectric phase copolymer nanopillars with good crystallinity without any further annealing procedure.

The piezoelectric and ferroelectric properties of the imprinted copolymer nanopillars were examined by PFM.[50] As is shown in Fig. 3a, the local PFM switching spectroscopy has been performed on two randomly chosen nanopillars and on the regions around them. The difference in piezoresponse between the copolymer nanopillars and the regions around them is striking – the piezoresponse amplitude loops on the copolymer nanopillars have large, distinct "butterfly" shapes (Fig. 3b), while the phase switches abruptly between opposing polarization states (Fig. 3c). The steep slopes in the phase near +7.5 V and −6 V and steady PFM amplitude after each switching cycle confirmed that the copolymer nanopillars had very stable, switchable ferroelectric polarization.[51] The regions around the nanopillars (circles in Fig. 3a), in contrast, shows no evidence of hysteresis, as shown in Fig. 3d and e, suggesting that there is no ferroelectric layer there. This conclusion is consistent with the previous SEM and AFM measurements showing no residual layer around the copolymer nanopillars.

The hysteresis loops shown in Fig. 3c exhibit a slight horizontal shift of approximately 1 V toward positive voltage, which is likely due to the difference of the work functions between the Pt coating on the PFM tip and the ITO bottom reference electrode. From the hysteresis loops, the copolymer nanopillars have a coercive field of approximately 67 MV m^{-1}. The coercive field value is within the range of 50 to 90 MV m^{-1} from previous studies of direct imprinted nanostructures on rigid substrates[7,18,52] and continuous spun film with similar thickness.[52] The coercive field could be further reduced with an enhanced crystallinity, for instance, previous study by Hu *et al.* has reported a coercive field of 10 MV m^{-1} in ferroelectric copolymer nanostructures by direct NIL with an optimized crystallinity.[5]

The ferroelectric nanopillars on flexible substrates could be used as nonvolatile memory cells for light weight and flexible data storage devices. To demonstrate this concept and possibility, we carried out the local switching study with four nanopillars from a randomly chosen 1.5 μm × 1.5 μm region. The writing and reading processes were performed by applying positive or negative voltages through the conductive AFM tip and followed by PFM scanning over the pillars. The results are shown in Fig. 4. An initial vertical displacement PFM image, recorded before field application showed weak PFM amplitude and phase signals (Fig. 4b and c). Then, the polymer was poled at the four locations indicated by the black dots and circles in Fig. 4d by positioning the AFM tip in contact with the polymer and applying a DC voltage of +20 V for 3 seconds on black dots and −20 V for 3 seconds on black circles. The PFM images (Fig. 4e and f) recorded after positive and negative poling showed newly formed irregular regions appearing with bright color in the amplitude image of the nanopillars (Fig. 4e) and with sharp contrast in the phase image (Fig. 4f). The white color regions in the upper two pillars in Fig. 4f correspond to the switched single

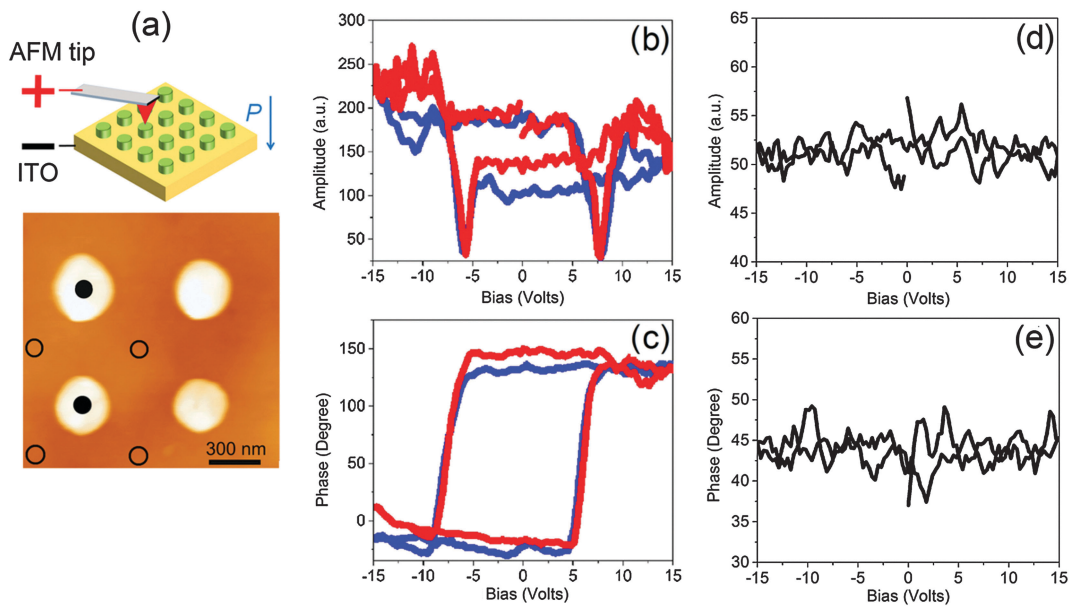

Fig. 3 (a) Piezoresponse hysteresis loops measurement taken at positions on top of the nanopillars (black dots) and at multiple positions around the pillars (black circles) with AFM tip as top electrode and ITO as bottom electrode. (b) and (c) Amplitude and phase PFM hysteresis loops taken on top of the two nanopillars. (d) and (e) Phase and amplitude PFM loops taken at four positions around the nanopillars (result for only one position is shown).

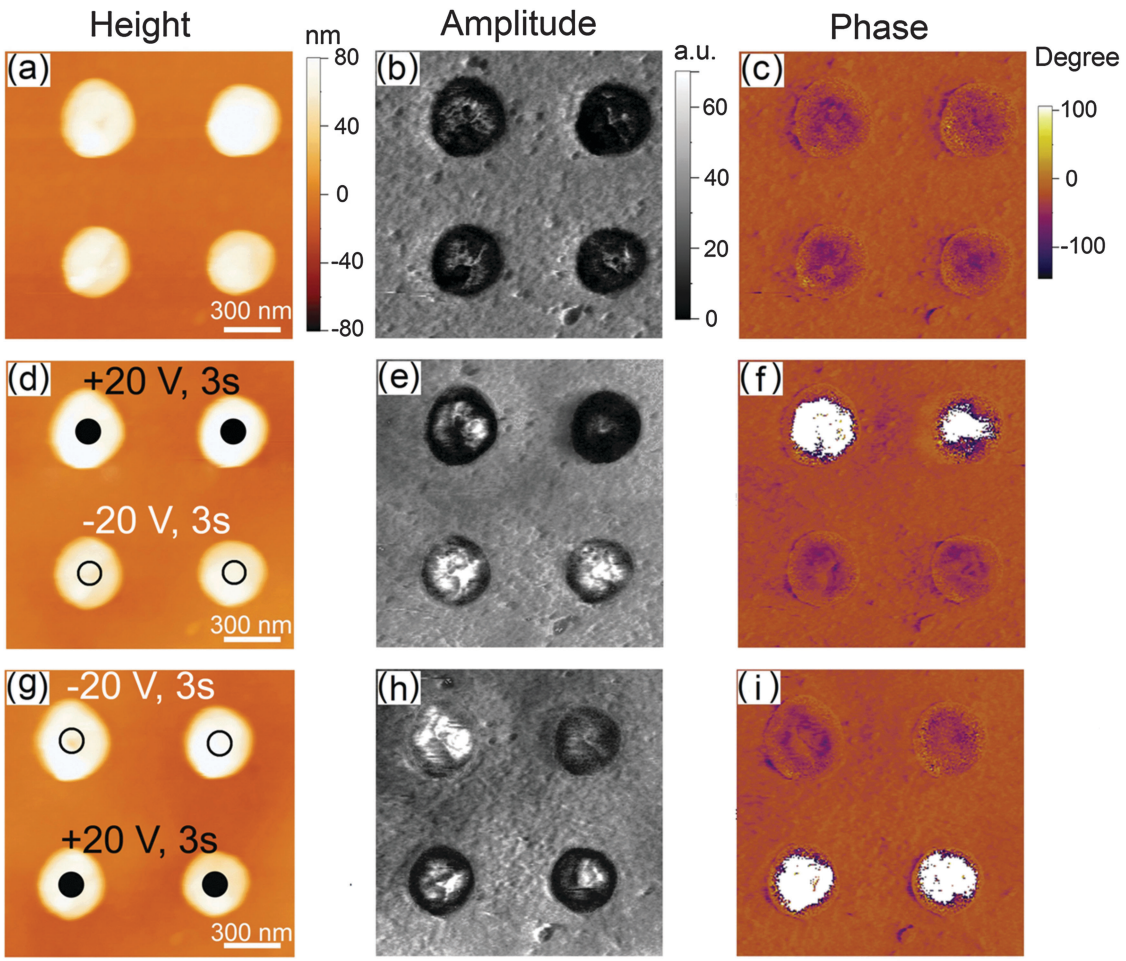

Fig. 4 (a)–(c) PFM height, amplitude and phase image of the four nanopillars before the PFM-tip local switching experiment. (d)–(f) PFM height, amplitude and phase images of the PFM measurement with +20 V poling for 3 s at the black dots indicated position and −20 V poling for 3 s at the black circles indicated position on (d). (g)–(i) PFM height, amplitude and phase images of the PFM measurement with −20 V poling for 3 s at the black circles indicated position and +20 V poling for 3 s at the black dots indicated position on (g).

domain regions with downward polarization direction. The inverse phase contrast in the lower two pillars indicated that the initial polarization was oriented upward or out-of-plane. The same process was repeated with a DC voltage of −20 V applied for 3 seconds at the black circles and +20 V applied for 3 seconds at the black dots in Fig. 4g, followed by PFM imaging (Fig. 4h and i). The regions around the four poling spots clearly reversed in phase, compared to the previous poling state in Fig. 4f. Enhancement of the PFM amplitude signal after positive poling in Fig. 4h is an illustration of more complete poling of the P(VDF–TrFE) in comparison to its as-grown state.[53]

From the local switching experiment we observed that the polarization switching with the copolymer nanopillars was very uniform, and no cross-talk between adjacent pillars was detected due to the removal of the residual layer.[20] The writing and reading processes did not cause any change to the morphology of the nanopillars, and single domain regions with stable and reversible polarization could be created. If each polarized nanopillar could be considered as one bit of information, the P(VDF–TrFE) nanopillars would yield a storage density of 1.6 Gb inch^{-2}. Although the data storage density is smaller than the values of 33 Gb inch^{-2} and 75 Gb inch^{-2} from previous reports with pretreated expensive hard mold and hard substrates,[5,7] the data density could be further improved by using higher density molds.

In order to confirm the scalability and macroscopic ferroelectric behavior of the copolymer nanopillars averaged over a larger area, we fabricated multilayer capacitors with layer sequence of Al/terpolymer/nanopillar/Pt/PET from top to bottom from the nanopillar array samples with a hexagonal arrangement by overcoating them with a terpolymer insulation layer and aluminum top electrode. The polarization was probed by measuring the pyroelectric response with a 2 mm-diameter beam using the Chynoweth method,[46] as in shown in Fig. 5a. Hysteresis loops were obtained by recording the signal as a function of sample bias, as is shown in Fig. 5b, for a range of DC bias voltages between ±40 V. Since the pyroelectric response is proportional to the net polarization,[47] the pyroelectric hysteresis loop (Fig. 5b) has the same shape as the polarization hysteresis loop. The good saturation and near rectangular shape of the

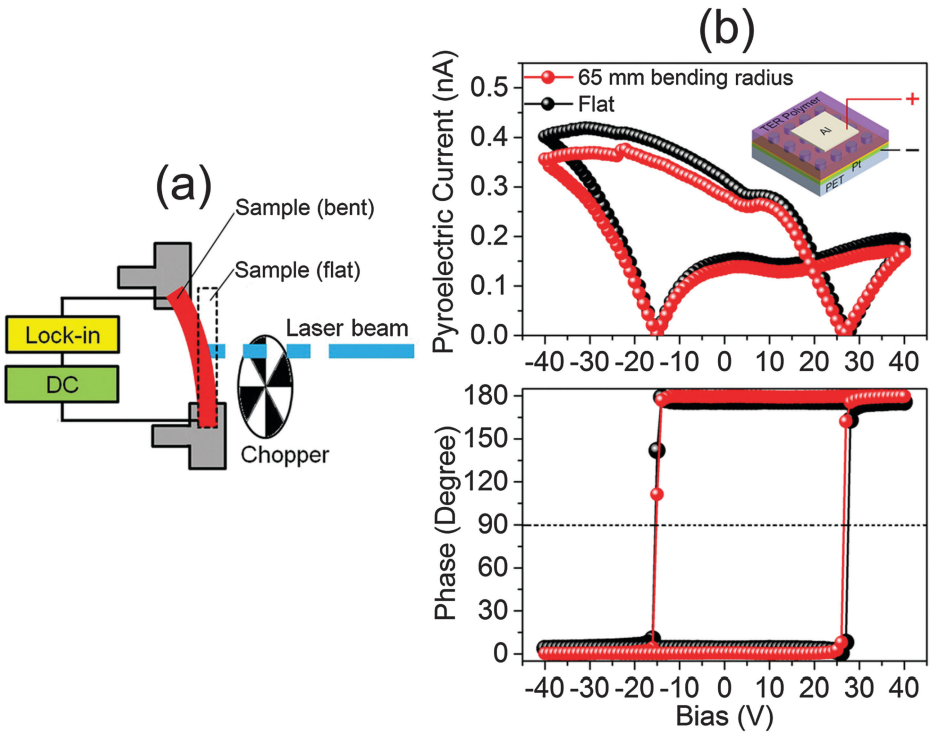

Fig. 5 (a) The pyroelectric hysteresis loop measurement setup. (b) The structure of the multilayer capacitors with layer sequence of Al/terpolymer/nanopillar/Pt/PET (inserted picture) and amplitude and phase curves of the pyroelectric hysteresis loop measured on the multilayer capacitor.

phase hysteresis loop indicated the P(VDF–TrFE) nanopillars have very stable and switchable ferroelectric polarization states. The effective coercive voltage of the copolymer nanopillar was 12.6 ± 0.2 V, and the calculated effective coercive field was 140 MV m^{-1} based on the AFM and finite element modeling results of the nanopillar capacitor (see ESI†). The higher coercive field comparing with the previous PFM study of the copolymer nanopillar arrays could be due to the uncertainty in the terpolymer film thickness and dielectric constant, and the different sample structures and measurement conditions. In the PFM measurement, a larger and nonuniform local electric field was achieved within the nanopillar region around the PFM tip,[36,54] therefore a lower coercive field could be acquired. It would be more reasonable to compare the calculated coercive field of the nanopillar capacitor with the values of copolymer LB or spun film capacitor samples, which normally have coercive fields around 90 to 110 MV m^{-1} with approximately 100 nm film thickness.[52,55]

As is shown in Fig. 5a, the multilayer capacitor sample was bent on a sample holder with a 65 mm convex bending radius while pyroelectric hysteresis loop measurements were performed under the same conditions. From the red curves in Fig. 5b, we observed no significant change of the pyroelectric signal or switching from the capacitor. The multilayer capacitor showed clear ferroelectric switching and reliable performance under a 65 mm bending radius. In addition, previous work with flexible P(VDF–TrFE) thin film devices has demonstrated working bending radius smaller than 20 mm.[14] Cracking or degradation of the large area Al and Pt electrodes could be the main factors that limit the bending radius of the flexible nanopillar capacitor sample.[56,57]

Conclusions

We have prepared arrays of ferroelectric polymer nanopillars directly on flexible substrates by using PDMS soft-mold based reverse NIL at low pressures. The results demonstrate that the arrays were faithful and uniform replicas of the PDMS mold, extending over large areas of at least 200 μm × 200 μm, with no detectable residual layer. The nanopillars were found to have good overall crystallinity with uniform (110) crystal orientation, and showed to be ferroelectric, exhibiting switchable and bi-stable piezoelectric and pyroelectric responses. The reverse NIL method described here is a high-yield, low cost, scalable, and highly customizable method that provides a promising alternative to the traditional rigid-mold direct nanoimprinting processes. This method may serve as a significant basis for future studies of 3D functional polymer nanostructures for flexible electronics, electro-mechanics and energy harvesting applications. There is still room for improvement, however. For example, higher density PDMS molds with smaller features could be developed for producing smaller size P(VDF–TrFE) nanopillars with higher density.[5,7] In addition, it would be interesting to explore the possibility of using spin-coating technique to coat polymer film on the soft mold. A few technical problems may need to be improved to get better results. For instance, in order to reduce or remove the polymer

residual layer, the film coated on the mold need to be thin enough such that little or no excess polymer exists after the polymer filling the mold cavities during the imprinting process. Furthermore, the ferroelectric properties and the switching of the nanopillar array on flexible substrates under larger strain need to be addressed for further study and applications.

Acknowledgements

This work was supported by a Faculty Seed grant from the UNL Research Council and by the National Science Foundation (NSF) through grant #ECCS-1201384 and though the Nebraska Materials Research Science and Engineering Center (MRSEC) under Grant No. DMR-1420645 (for PFM electrical characterization).

References

1 R. G. Cai, H. G. Kassa, A. Marrani, A. J. J. M. van Breemen, G. H. Gelinck, B. Nysten, Z. J. Hu and A. M. Jonas, *Appl. Phys. Lett.*, 2014, **105**, 113113.
2 T. Sharma, S. Naik, J. Langevine, B. Gill and J. X. J. Zhang, *IEEE Trans. Biomed. Eng.*, 2015, **62**, 188–195.
3 K. J. Kim and S. Tadokoro, *Electroactive polymers for robotic applications: artificial muscles and sensors*, Springer, London, 2007.
4 H. Xu, Z.-Y. Cheng, D. Olson, T. Mai, Q. M. Zhang and G. Kavarnos, *Appl. Phys. Lett.*, 2001, **78**, 2360–2362.
5 Z. Hu, M. Tian, B. Nysten and A. M. Jonas, *Nat. Mater.*, 2009, **8**, 62–67.
6 S. J. Kang, I. Bae, Y. J. Shin, Y. J. Park, J. Huh, S. M. Park, H. C. Kim and C. Park, *Nano Lett.*, 2011, **11**, 138–144.
7 X. Z. Chen, Q. Li, X. Chen, X. Guo, H. X. Ge, Y. Liu and Q. D. Shen, *Adv. Funct. Mater.*, 2013, **23**, 3124–3129.
8 J. Y. Son, S. Ryu, Y. C. Park, Y. T. Lim, Y. S. Shin, Y. H. Shin and H. M. Jang, *ACS Nano*, 2010, **4**, 7315–7320.
9 C. E. Chang, V. H. Tran, J. B. Wang, Y. K. Fuh and L. W. Lin, *Nano Lett.*, 2010, **10**, 726–731.
10 L. Persano, C. Dagdeviren, Y. W. Su, Y. H. Zhang, S. Girardo, D. Pisignano, Y. G. Huang and J. A. Rogers, *Nat. Commun.*, 2013, **4**, 1633.
11 J.-H. Lee, H.-J. Yoon, T. Y. Kim, M. K. Gupta, J. H. Lee, W. Seung, H. Ryu and S.-W. Kim, *Adv. Funct. Mater.*, 2015, **25**, 3203–3209.
12 Y. K. Fuh, P. C. Chen, Z. M. Huang and H. C. Ho, *Nano Energy*, 2015, **11**, 671–677.
13 Z. M. Dang, J. K. Yuan, S. H. Yao and R. J. Liao, *Adv. Mater.*, 2013, **25**, 6334–6365.
14 S. K. Hwang, I. Bae, R. H. Kim and C. Park, *Adv. Mater.*, 2012, **24**, 5910–5914.
15 R. Li, C. X. Xiong, D. L. Kuang, L. J. Dong, Y. A. Lei, J. L. Yao, M. Jiang and L. B. Li, *Macromol. Rapid Commun.*, 2008, **29**, 1449–1454.
16 Q. D. Ling, D. J. Liaw, C. X. Zhu, D. S. H. Chan, E. T. Kang and K. G. Neoh, *Prog. Polym. Sci.*, 2008, **33**, 917–978.
17 L. Zhang, S. Ducharme and J. Li, *Appl. Phys. Lett.*, 2007, **91**, 172906.
18 Y. M. Liu, D. N. Weiss and J. Y. Li, *ACS Nano*, 2010, **4**, 83–90.
19 J. R. Fang, Z. K. Shen, S. Yang, Q. Lu, J. X. Li, Y. F. Chen and R. Liu, *Microelectron. Eng.*, 2011, **88**, 2033–2036.
20 H. G. Kassa, R. G. Cai, A. Marrani, B. Nysten, Z. J. Hu and A. M. Jonas, *Macromolecules*, 2013, **46**, 8569–8579.
21 D. E. Martinez-Tong, M. Soccio, M. C. Garcia-Gutierrez, A. Nogales, D. R. Rueda, N. Alayo, F. Perez-Murano and T. A. Ezquerra, *Appl. Phys. Lett.*, 2013, **102**, 191601.
22 I. M. W. a. P. R. Pinnock, *Br. J. Appl. Phys.*, 1966, **17**, 3.
23 V. Zardetto, T. M. Brown, A. Reale and A. Di Carlo, *J. Polym. Sci., Part B: Polym. Phys.*, 2011, **49**, 638–648.
24 M. Peter, F. Furthner, J. Deen, W. J. M. de Laat and E. R. Meinders, *Thin Solid Films*, 2009, **517**, 3081–3086.
25 P. F. Moonen, I. Yakimets and J. Huskens, *Adv. Mater.*, 2012, **24**, 5526–5541.
26 H. Lee, S. H. Hong, K. Y. Yang and K. W. Choi, *Appl. Phys. Lett.*, 2006, **88**, 143112.
27 C. Wang, Q. F. Xia, W. D. Li, Z. L. Fu, K. J. Morton and S. Y. Chou, *Small*, 2010, **6**, 1242–1247.
28 I. Park, S. H. Ko, H. Pan, C. P. Grigoropoulos, A. P. Pisano, J. M. J. Frechet, E. S. Lee and J. H. Jeong, *Adv. Mater.*, 2008, **20**, 489–496.
29 H. Schift, *J. Vac. Sci. Technol., B: Microelectron. Nanometer Struct.–Process., Meas., Phenom.*, 2008, **26**, 458–480.
30 H. Yoon, H. Lee and W. B. Lee, *Korea-Aust. Rheol. J.*, 2014, **26**, 39–48.
31 D. Hegemann, H. Brunner and C. Oehr, *Nucl. Instrum. Methods Phys. Res., Sect. B*, 2003, **208**, 281–286.
32 X. D. Huang, L. R. Bao, X. Cheng, L. J. Guo, S. W. Pang and A. F. Yee, *J. Vac. Sci. Technol., B: Microelectron. Nanometer Struct.–Process., Meas., Phenom.*, 2002, **20**, 2872–2876.
33 J. Song, H. Lu, S. Li, L. Tan, A. Gruverman and S. Ducharme, *Nanotechnology*, 2016, **27**, 015302.
34 X. M. Zhao, Y. N. Xia and G. M. Whitesides, *J. Mater. Chem.*, 1997, **7**, 1069–1074.
35 J. J. Dumond, H. Y. Low, H. P. Lee and J. Y. H. Fuh, *Mater. Horiz.*, 2016, **3**, 152–160.
36 H. Fang, Q. Yan, C. Geng, N. Y. Chan, K. Au, J. Yao, S. M. Ng, C. W. Leung, Q. Li, D. Guo, H. L. Wa Chan and J. Dai, *J. Appl. Phys.*, 2016, **119**, 014104.
37 D. Qin, Y. N. Xia and G. M. Whitesides, *Nat. Protoc.*, 2010, **5**, 491–502.
38 H. Yoon, S. H. Lee, S. H. Sung, K. Y. Suh and K. Char, *Langmuir*, 2011, **27**, 7944–7948.
39 S. Ducharme, S. P. Palto and V. M. Fridkin, in *Ferroelectric and Dielectric Thin Films*, ed. H. S. Nalwa, Academic Press, San Diego, 2002, vol. 3, pp. 545–591.
40 J. Song, H. Lu, A. Gruverman and S. Ducharme, *Appl. Phys. Lett.*, 2014, **104**, 192901.
41 M. J. Bai and S. Ducharme, *Appl. Phys. Lett.*, 2004, **85**, 3528–3530.
42 S. Poddar and S. Ducharme, *Appl. Phys. Lett.*, 2013, **103**, 202901.
43 B. J. Chu, X. Zhou, B. Neese, Q. M. Zhang and F. Bauer, *IEEE Trans. Dielectr. Electr. Insul.*, 2006, **13**, 1162–1169.

44 J. L. Wang, X. J. Meng, S. Z. Yuan, J. Yang, J. L. Sun, H. S. Xu and J. H. Chu, *Appl. Phys. Lett.*, 2008, **93**, 192905.
45 R. W. Cheary and A. Coelho, *J. Appl. Crystallogr.*, 1992, **25**, 109–121.
46 A. Bune, S. Ducharme, V. Fridkin, L. Blinov, S. Palto, N. Petukhova and S. Yudin, *Appl. Phys. Lett.*, 1995, **67**, 3975–3977.
47 A. V. Bune, C. X. Zhu, S. Ducharme, L. M. Blinov, V. M. Fridkin, S. P. Palto, N. G. Petukhova and S. G. Yudin, *J. Appl. Phys.*, 1999, **85**, 7869–7873.
48 S. Y. Chou, *U.S. Pat.*, 63095802001.
49 J. Choi, C. N. Borca, P. A. Dowben, A. Bune, M. Poulsen, S. Pebley, S. Adenwalla, S. Ducharme, L. Robertson, V. M. Fridkin, S. P. Palto, N. N. Petukhova and S. G. Yudin, *Phys. Rev. B: Condens. Matter Mater. Phys.*, 2000, **61**, 5760–5770.
50 D. A. Bonnell, S. V. Kalinin, A. L. Kholkin and A. Gruverman, *MRS Bull.*, 2009, **34**, 648–657.
51 S. Jesse, A. P. Baddorf and S. V. Kalinin, *Appl. Phys. Lett.*, 2006, **88**, 062908.
52 K. Kuniko and O. Hiroji, *Jpn. J. Appl. Phys.*, 1986, **25**, 383.
53 A. Gruverman and A. Kholkin, *Rep. Prog. Phys.*, 2006, **69**, 2443–2474.
54 S. V. Kalinin, E. Karapetian and M. Kachanov, *Phys. Rev. B: Condens. Matter Mater. Phys.*, 2004, **70**, 184101.
55 S. Ducharme, V. M. Fridkin, A. V. Bune, S. P. Palto, L. M. Blinov, N. N. Petukhova and S. G. Yudin, *Phys. Rev. Lett.*, 2000, **84**, 175–178.
56 H. Chai, *Int. J. Solids Struct.*, 2011, **48**, 1092–1100.
57 Z. H. Cao, K. Hu and X. K. Meng, *Mater. Sci. Eng., A*, 2012, **536**, 244–248.

Supporting Information

Ferroelectric polymer nanopillars arrays on flexible substrate by reverse nanoimprint lithography

Jingfeng Song,[1] Haidong Lu,[1] Keith Foreman[1], Shumin Li,[2] Li Tan,[2] Shireen Adenwalla,[1]Alexei Gruverman[1] and Stephen Ducharme[1]

[1]Department of Physics and Astronomy & Nebraska Center for Materials and Nanoscience, University of Nebraska, Lincoln, NE 68588-0299, USA

[2]Department of Mechanical and Materials Engineering & Nebraska Center for Materials and Nanoscience, University of Nebraska, Lincoln, NE 68588-0526, USA

Pressure measurement

We used the Omega Universal Load Cell to measure the pressure applied onto our sample during the reverse nanoimprint lithography process through the SPECAC hydraulic press system. Since the imprinting temperature of 135 °C is beyond the working temperature of the Load Cell, we recorded the pressure-time curve at 25 °C, which is shown in Fig. S**1**. The initial pressure of 3 bar slowly decreased to 2.6 bar after 60 minutes, and to 2.2 bar after another 90 minutes when the pressure was manually released. The exactly same starting pressure of 3 bar was used when doing our reverse nanoimprint lithography experiment at 135 °C, the pressure value could be slightly different from 2.6 bar over 60 minutes. The reason for the pressure decrease may be due to the relaxation of the sample and limitation of the design of the hydraulic press system to hold a small pressure for extended period of time.

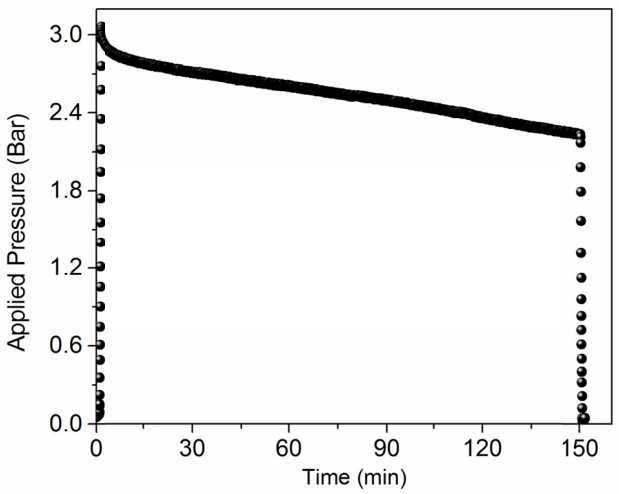

Figure S1. The pressure applied onto the sample during the reverse nanoimprint lithography process with respect to time measured at 25 °C.

Nanopillar array with hexagonal arrangement

The soft mold based low-pressure reverse nanoimprint lithography is also highly customizable based on the initial silicon nanostamps chosen. By choosing a hexagonal arranged silicon nanostamp to prepare our PDMS soft molds, we were also able to fabricate large area, uniform P(VDF-TrFE) nanopillars on a PET substrate with hexagonal arrangements as is shown in Fig. S2. The copolymer nanopillars are 99 ± 3 nm in height, 676 ± 8 nm in period, and an average of 250 ± 6 nm from the top and bottom widths as measured from the AFM 3D topography and line scan in Fig. S2. The sizes and periodicity of the nanopillars were very close to the copolymer nanopillars in the rectangular arrangement shown in Fig. 2a.

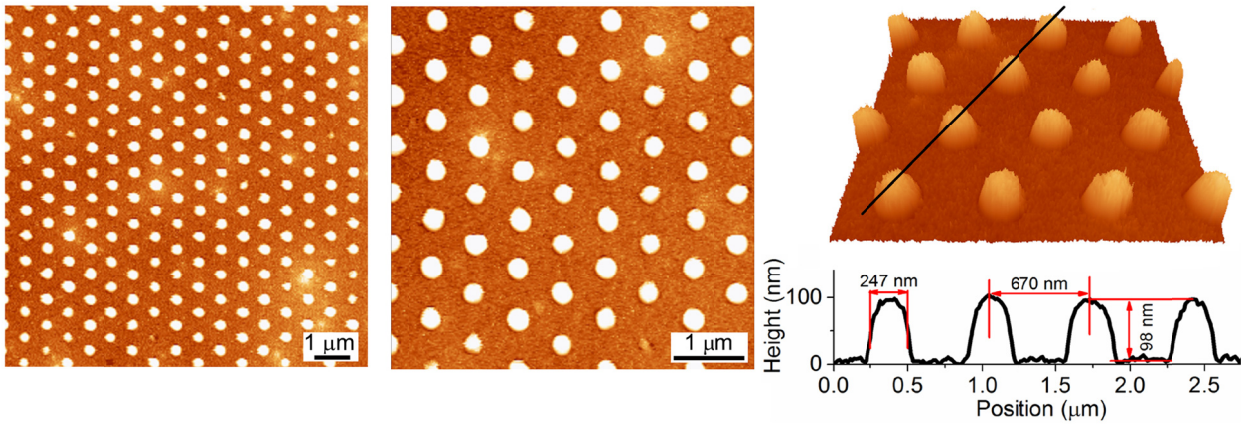

Figure S2. AFM topography of the P(VDF-TrFE) nanopillars with hexagonal arrangements and the line scan profile along the black line indicated on the 3D topography image.

Langmuir-Blodgett deposition of terpolymer capping layer

The terpolymer of vinylidene fluoride (55.8%), trifluoroethylene (35%), and chlorofluoroethylene (9.2%) or P(VDF-TrFE-CFE), from Kunshan Hisense Electronics Co., Ltd., was used as received and dissolved in dimethylsulfoxide to a concentration of 0.05% by weight. The thin film of 45 nominal monolayers was transferred to the sample surface by horizontal Langmuir-Blodgett (LB) deposition at a surface pressure of 10 mN/m. The method of sample preparation and the properties of produced films are described in greater detail elsewhere.[1]

Calculation of effective coercive voltage of nanopillars

Since polarization reversal occurs at the coercive field[2] and the polarization reversed when the phase value was close to 90°. In order to calculate the effective coercive voltage of the copolymer nanopillars in the multilayer capacitors, we first acquired the polarization reversal voltages of –15.4 ± 0.25 V and 26.5 ± 0.3 V, respectively, by inspecting the x-intercepts of the

phase diagram with a horizontal line at 90° phase (dashed line in Fig. 5b). From the half-width of the phase loop, we calculated the coercive voltage of the nanopillar capacitor V_c to be 21.0 ± 0.3 V. The approximate 5 V shift of the coercive voltage to the negative voltage direction and asymmetric curves could be due to the difference of the work function of electrodes and asymmetric electric contact of the ferroelectric polymer with the top and bottom electrodes.[3, 4] The 45 ML terpolymer insulation layer was the main cause of the coercive voltage increase, as shown below. The AFM topography of the terpolymer coated nanopillars with hexagonal arrangement is shown in Fig. S3a, with the corresponding line scans of the nanopillars and terpolymer coating illustrated in Fig. S3b. The copolymer nanopillar, terpolymer coating and aluminum top electrode is indicated with green, yellow and gray color respectively in Fig. S3b. The finite element modeling (FEM) results of the applied voltage distribution over the nanopillars using Maxwell software are shown in Fig. S3c. The thickness of the 45 ML terpolymer layer is 180 nm with 4 nm per monolayer.[5] The thickness of the copolymer nanopillar layer is 90 nm according to previous AFM measurements. The dielectric constant of the copolymer is 10,[6] and the dielectric constant of terpolymer is 50.[7, 8] The much higher dielectric constant of the terpolymer is beneficial for obtaining a higher voltage drop across the ferroelectric copolymer layer. The applied voltage distribution across the center of a pillar (indicated with a white dashed line in Fig. S3c) is illustrated in Fig. S3d. The voltage drop across the copolymer nanopillar according to the modeling calculation is 24 V, which is 60% of the applied 40 V voltage. Based on the proportionality of the voltage drop across the nanopillar and the applied voltage in modeling result, the effective coercive voltage of the copolymer nanopillar $V_c(\text{eff}) = Vc \times 60\%$ was 12.6 ± 0.2 V.

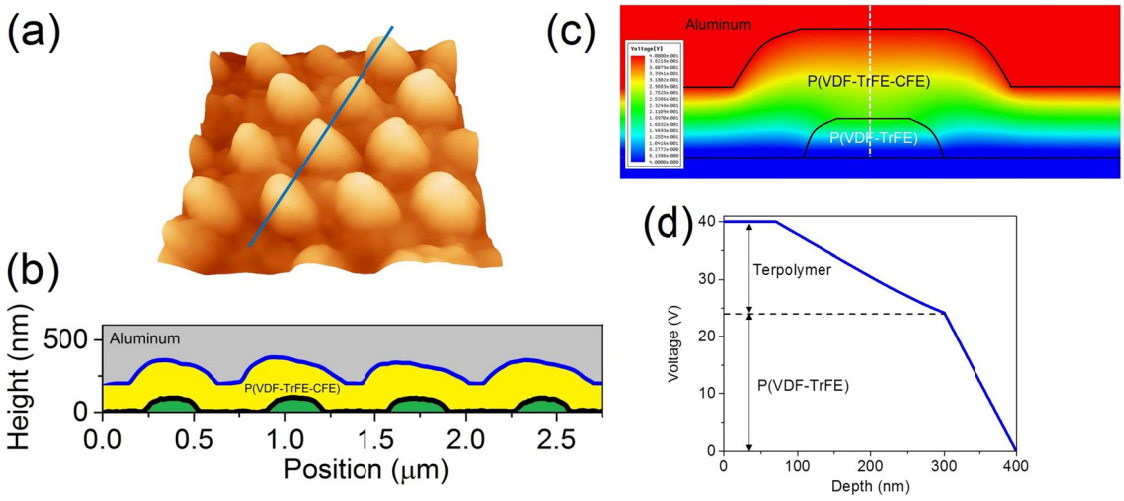

Figure S3. (a) AFM topography of the terpolymer coated P(VDF-TrFE) nanopillars. (b) Comparison of the AFM line scan result of nanopillar (black curve) and terpolymer coated nanopillar (blue curve). (c) Voltage drop distribution over the aluminum/terpolymer/nanopillar multilayer region with FEM method. (d) Voltage drop along the white dashed line in (c).

References

1. S. Poddar and S. Ducharme, *Appl Phys Lett*, 2013, **103**, 202901.
2. M. E. Lines and A. M. Glass, *Principles and applications of ferroelectrics and related materials*, Clarendon Press, Oxford Eng., 1977.
3. S. J. Kang, I. Bae, Y. J. Shin, Y. J. Park, J. Huh, S. M. Park, H. C. Kim and C. Park, *Nano Lett*, 2011, **11**, 138-144.
4. F. Xia and Q. M. Zhang, *Appl Phys Lett*, 2004, **85**, 1719-1721.
5. S. Poddar, K. Foreman, S. Adenwalla and S. Ducharme, *Appl Phys Lett*, 2016, **108**, 012908.
6. S. Ducharme, S. P. Palto and V. M. Fridkin, in *Ferroelectric and Dielectric Thin Films*, ed. H. S. Nalwa, Academic Press, San Diego, 2002, vol. 3, pp. 545-591.
7. B. J. Chu, X. Zhou, B. Neese, Q. M. Zhang and F. Bauer, *IEEE T Dielect El In*, 2006, **13**, 1162-1169.
8. J. L. Wang, X. J. Meng, S. Z. Yuan, J. Yang, J. L. Sun, H. S. Xu and J. H. Chu, *Appl Phys Lett*, 2008, **93**.